Supporting information

Heteroatom sulfur-doping in single-atom Fe-NC catalysts for durable oxygen reduction reaction in both alkaline and acidic media

Jin Yan[a], Tianyi Gu[a], Ruhua Shi[a], Xin Chen[b,*], Mark H Rümmeli[a,c], Ruizhi Yang [a,*]

[a] College of Energy, Soochow Institute for Energy and Materials Innovations, Soochow University, Suzhou 215006, China
E-mail: yangrz@suda.edu.cn

[b] Computational Chemistry and Molecular Simulation, College of Chemistry and Chemical Engineering, Southwest Petroleum University, Chengdu 610500, China
E-mail: chenxin830107@pku.edu.cn

[c] Centre of Polymer and Carbon Materials, Polish Academy of Sciences, M. Curie-Sklodowskiej 34, Zabrze 41-819, Poland
Institute of Environmental Technology, VŠB-Technical University of Ostrava, 17. Listopadu 15, Ostrava 708 33, Czech Republic

Fig. S1-S26

Table S1-S4

Theoretical calculations

The four-electron ORR mechanism in acid condition contains following steps:

$$* + O_2 + H^+ + e^- \rightarrow *OOH \quad (1)$$

$$*OOH + H^+ + e^- \rightarrow *O + H_2O \quad (2)$$

$$*O + H^+ + e^- \rightarrow *OH \quad (3)$$

$$*OH + H^+ + e^- \rightarrow * + H_2O \quad (4)$$

and the four-electron ORR mechanism in alkaline condition contains following steps:

$$* + O_2 + H_2O + e^- \rightarrow *OOH + OH^- \quad (5)$$

$$*OOH + e^- \rightarrow *O + OH^- \quad (6)$$

$$*O + H_2O + e^- \rightarrow *OH + OH^- \quad (7)$$

$$*OH + e^- \rightarrow * + OH^- \quad (8)$$

The binding energy (ΔE) of ORR intermediates on MN_4X_n is defined as follows:

$$\Delta E_{*OOH} = E_{*OOH} - E_{MN4Xn} - (2E_{H2O} - 3/2E_{H2}) \quad (9)$$

$$\Delta E_{*O} = E_{*O} - E_{MN4Xn} - (E_{H2O} - E_{H2}) \quad (10)$$

$$\Delta E_{*OH} = E_{*OH} - E_{MN4Xn} - (E_{H2O} - 1/2E_{H2}) \quad (11)$$

in which E_{*OOH}, E_{*O}, and E_{*OH} represents the overall energy of H-(S)-Fe-NC with adsorbed OOH, O, and OH, respectively. E_{H2O} and E_{H2} represents the energy of water molecule and hydrogen molecule, respectively. The smaller the ΔE value, the stronger the binding strength.

The adsorption free energy (ΔG_{ads}) is calculated based on the computational hydrogen electrode (CHE) model proposed by Nørskov and co-workers: $\Delta G_{ads} = \Delta E + \Delta ZPE - T\Delta S$. where ΔZPE, T, and ΔS is the change of zero-point energy, the temperature (298.15 K) and the change of entropy, respectively. According to the summary by Zhang et al., for the ORR species adsorbed on various catalysts, zero-point energy possesses similar value as the entropy. Therefore, the ΔG_{ads} can be expressed by:

$$\Delta G_{*OOH} = \Delta E_{*OOH} + 0.40 \quad (12)$$

$$\Delta G_{*O} = \Delta E_{*O} + 0.05 \quad (13)$$

$$\Delta G_{*OH} = \Delta E_{*OH} + 0.35 \quad (14)$$

The relationship between ΔG_{ads} and binding strength of ORR intermediates is similar

to that between ΔE and binding strength, that is, a small ΔG_{ads} value indicates a strong binding strength of intermediates.

The Gibbs free energy change for each step in four-electron pathway can be calculated by the following equations:

$$\Delta G_1 = \Delta G_{*OOH} - 4.92 - eU \quad (15)$$

$$\Delta G_2 = \Delta G_{*O} - \Delta G_{*OOH} - eU \quad (16)$$

$$\Delta G_3 = \Delta G_{*OH} - \Delta G_{*O} - eU \quad (17)$$

$$\Delta G_4 = -\Delta G_{*OH} - eU \quad (18)$$

where the U represents the applied electrode potential. When the U = 0 V, the overpotential of ORR (η^{ORR}) as the key descriptor of the ORR catalytic activity can be obtained by:

$$\eta^{ORR} = 1.23 + \max(\Delta G_1, \Delta G_2, \Delta G_3, \Delta G_4)/e \quad (19)$$

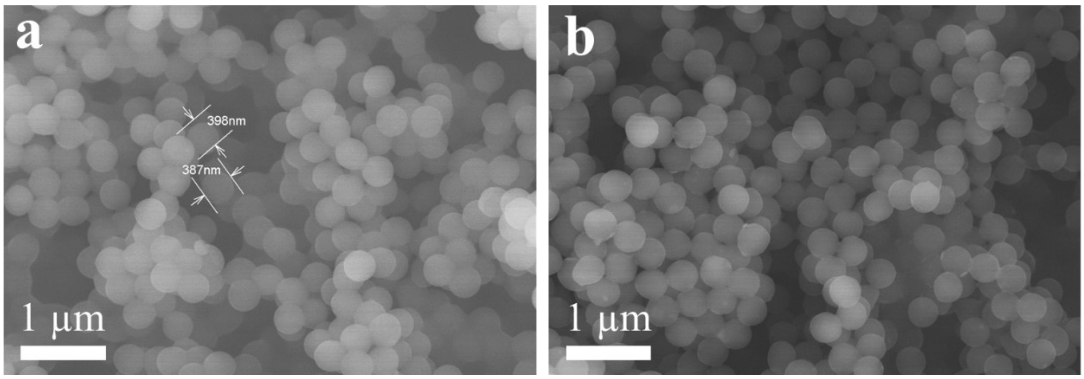

Fig S1. SEM image of (a) the PS and (b) the functionalized PS with PVP.

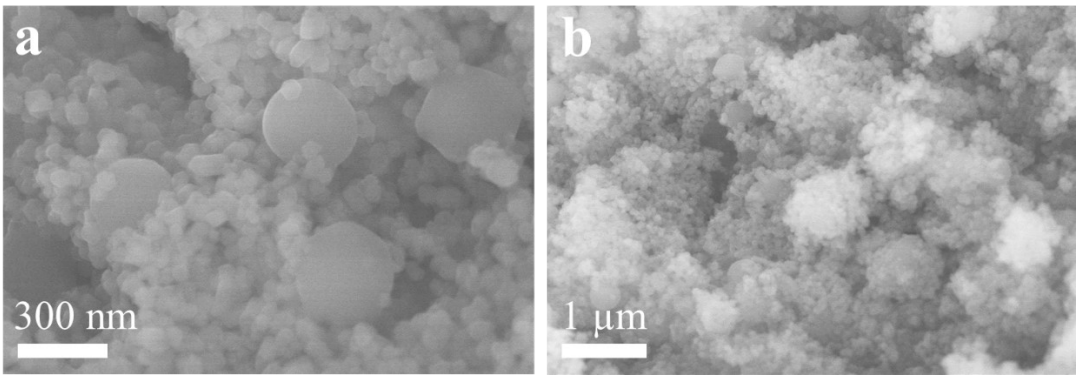

Fig S2. SEM image of PS@Fe-ZIF.

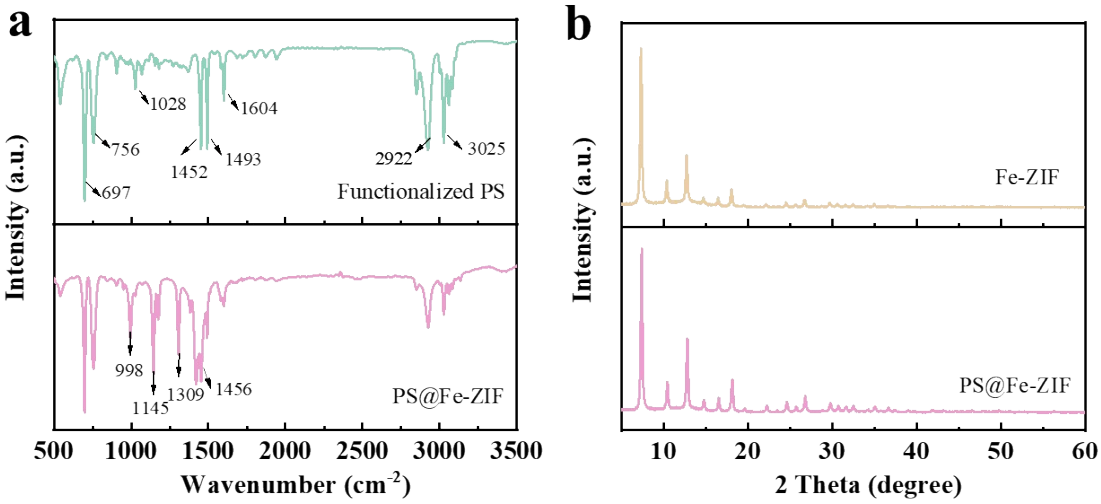

Fig S3. (a) FT-IR spectrum of functionalized PS and PS@Fe-ZIF. (b) XRD pattern of the Fe-ZIF precursor and PS@Fe-ZIF.

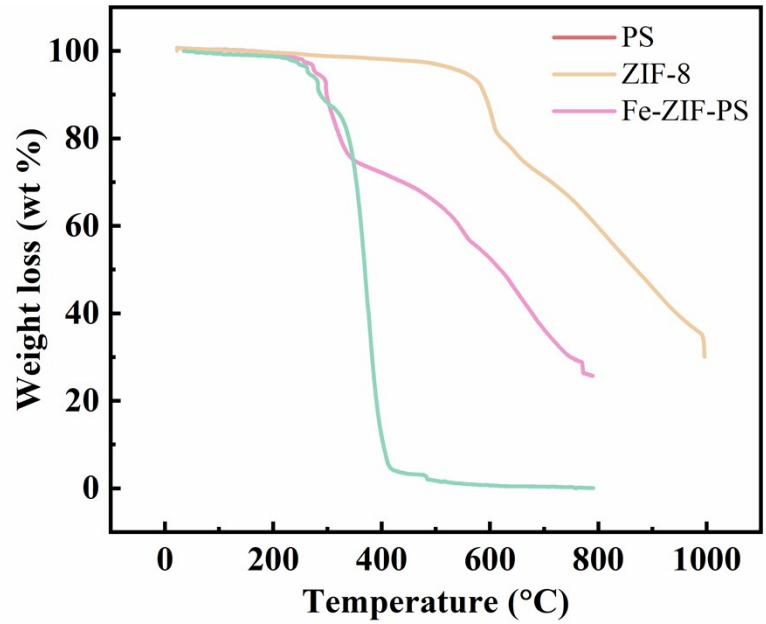

Fig S4. (a) TG spectrum of functionalized PS, Fe-ZIF precursor and PS@Fe-ZIF.

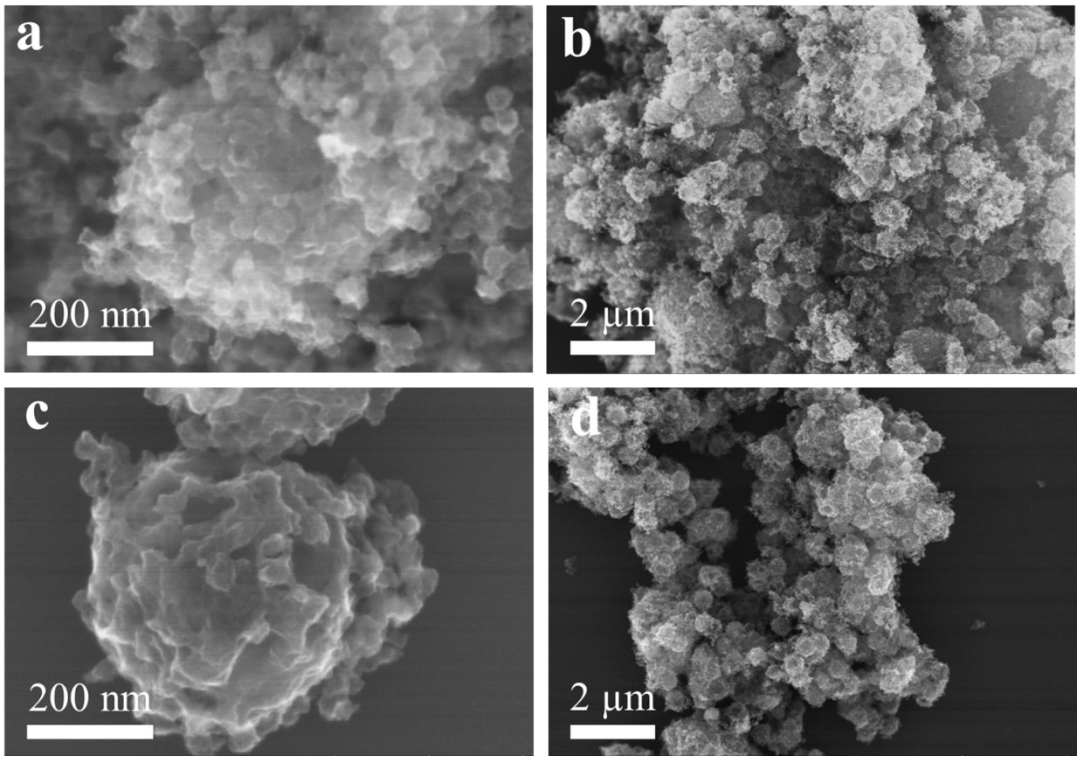

Fig S5. SEM image of (a-b) H-NC and (c-d) H-Fe-NC.

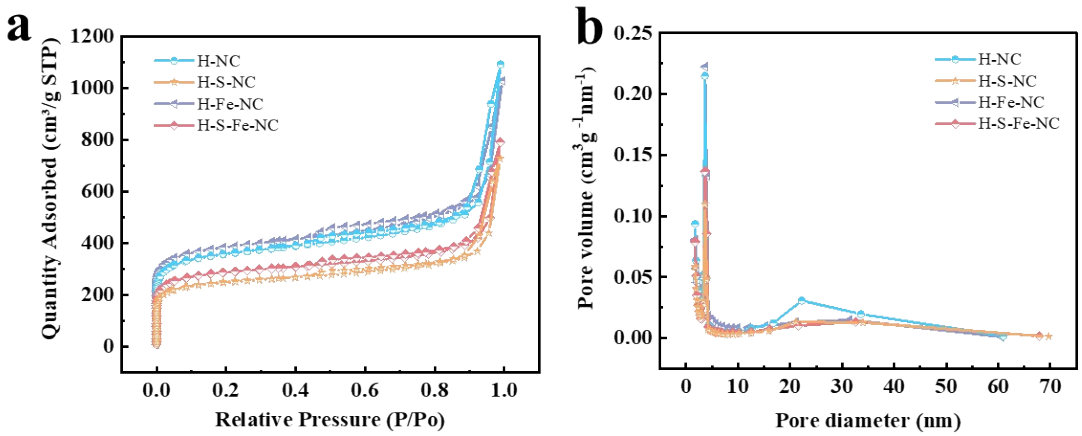

Fig S6. (a)N_2 adsorption/desorption isotherms and (b) pore size distribution of H-NC, H-S-NC, H-Fe-NC and H-S-Fe-NC.

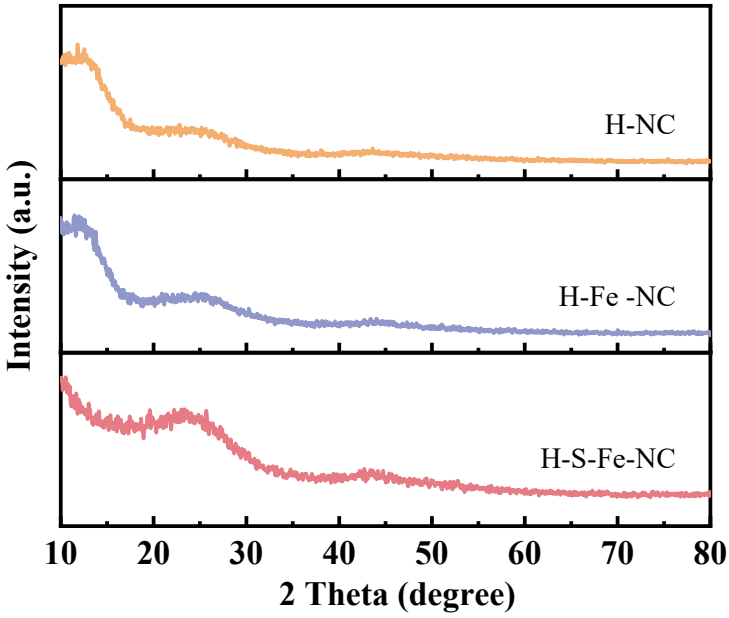

Fig S7. XRD pattern of H-NC, H-S-NC, H-Fe-NC and H-S-Fe-NC.

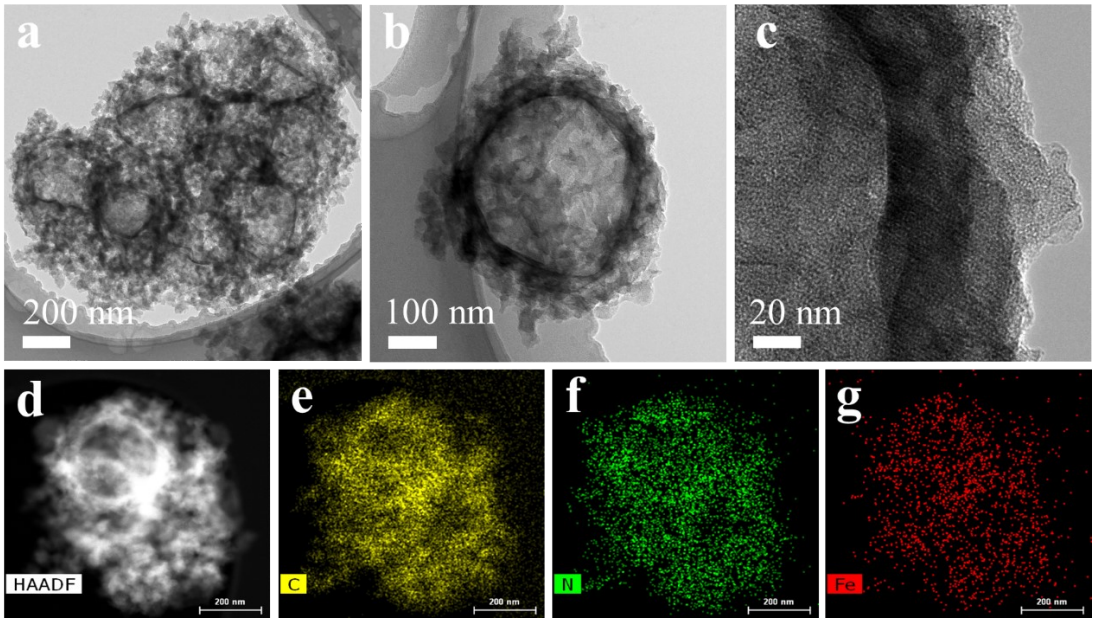

Fig S8. (a-b) TEM, (c) HR-TEM, (d) STEM image and corresponding elemental mappings of (e) C, (f) N and (g) Fe for H-Fe-NC.

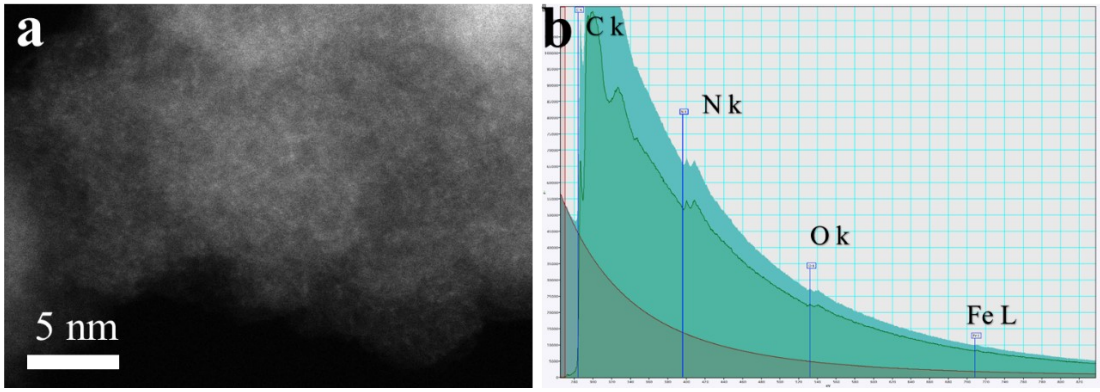

Fig S9. (a) HAADF-STEM image and (b) EELS spectrums of H-Fe-NC.

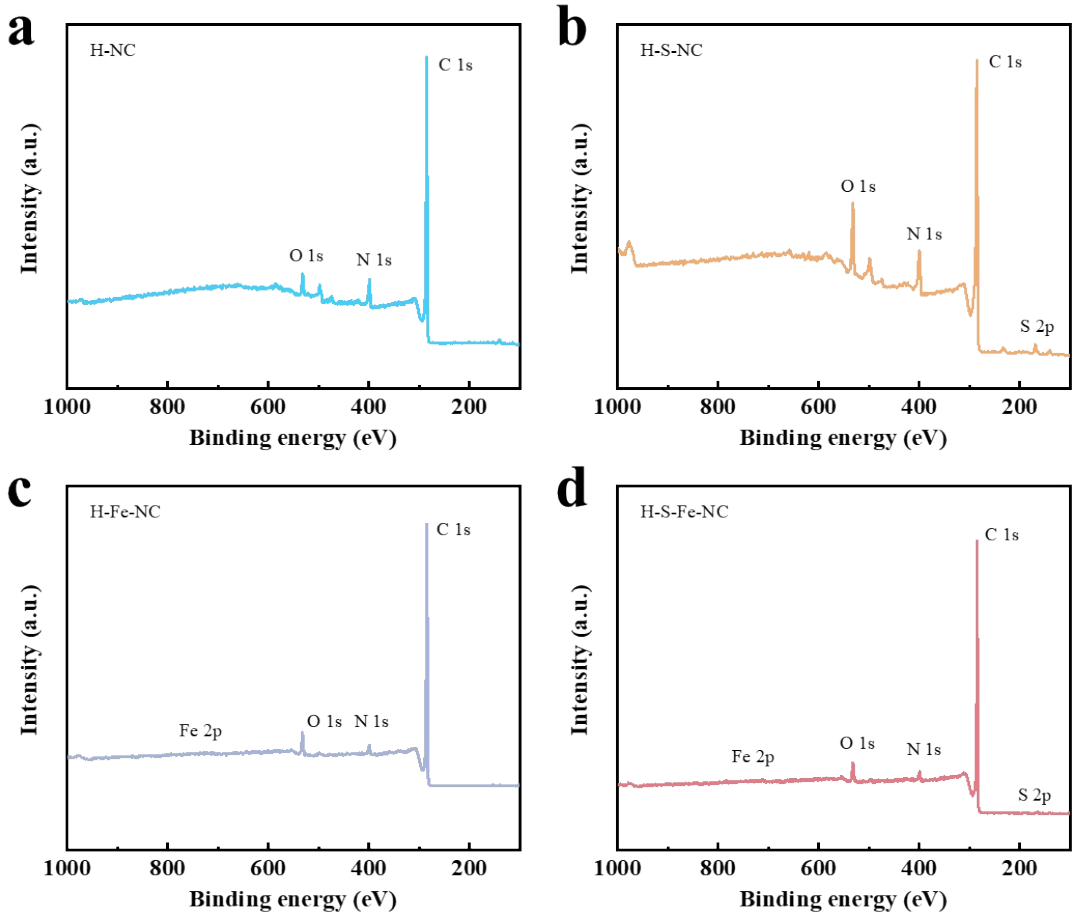

Fig S10. XPS survey of (a) H-NC, (b) H-S-NC, (c) H-Fe-NC and (d) H-S-Fe-NC.

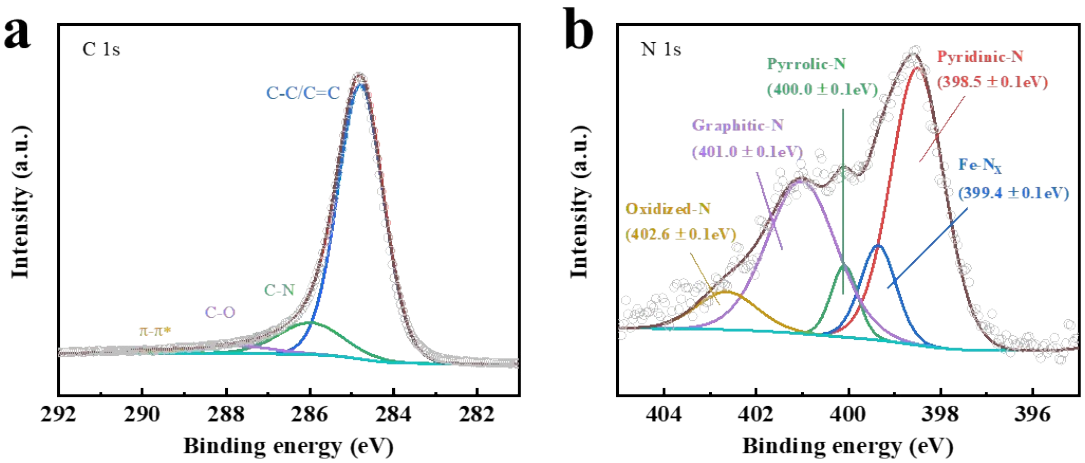

Fig S11. (a) High-resolution of C 1s and (b) N 1s XPS spectra of H-Fe-NC.

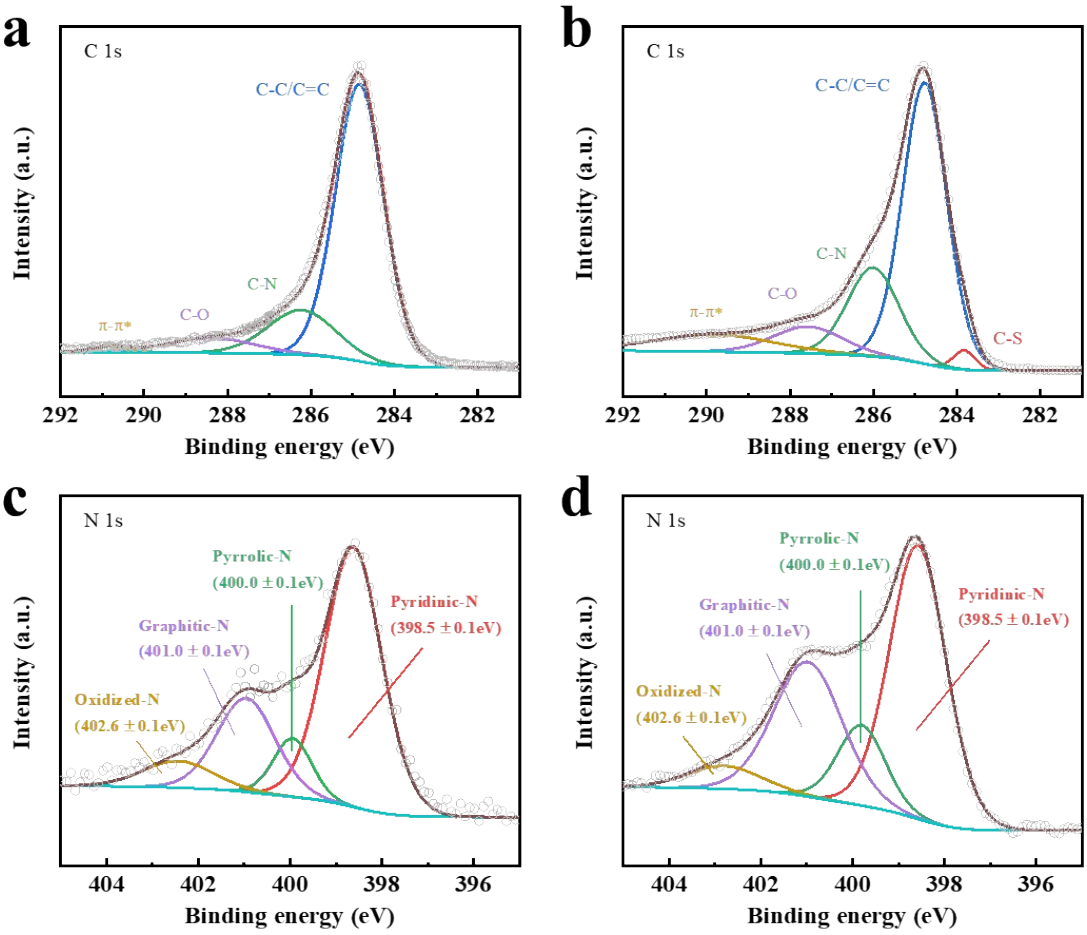

Fig S12. (a-b) High-resolution C 1s and (c-d) N 1s XPS spectra H-NC and H-S-NC respectively.

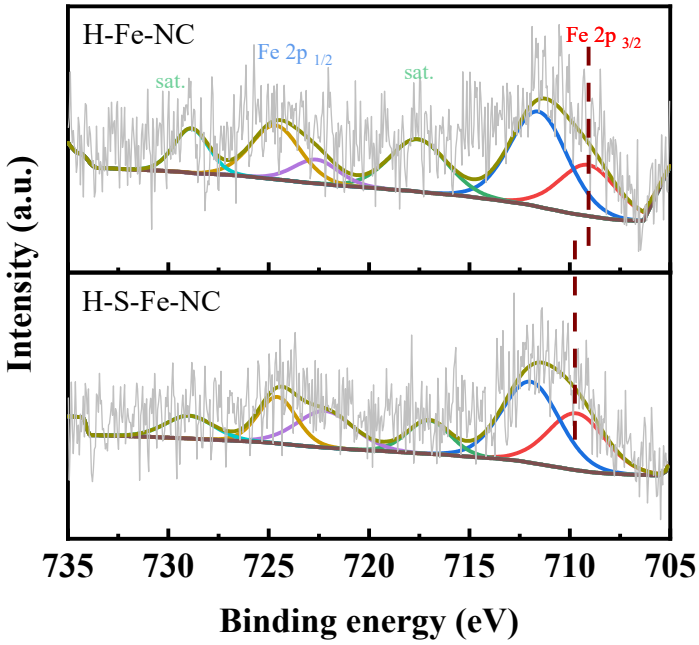

Fig S13. (a) High-resolution Fe 2p XPS spectra of H-Fe-NC and H-S-Fe-NC.

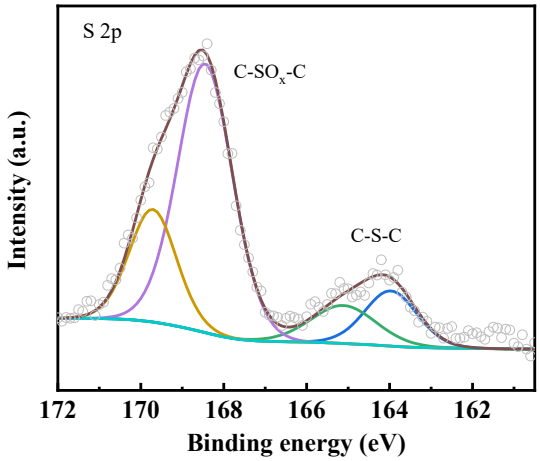

Fig S14. S 2p XPS spectra of H-S-NC.

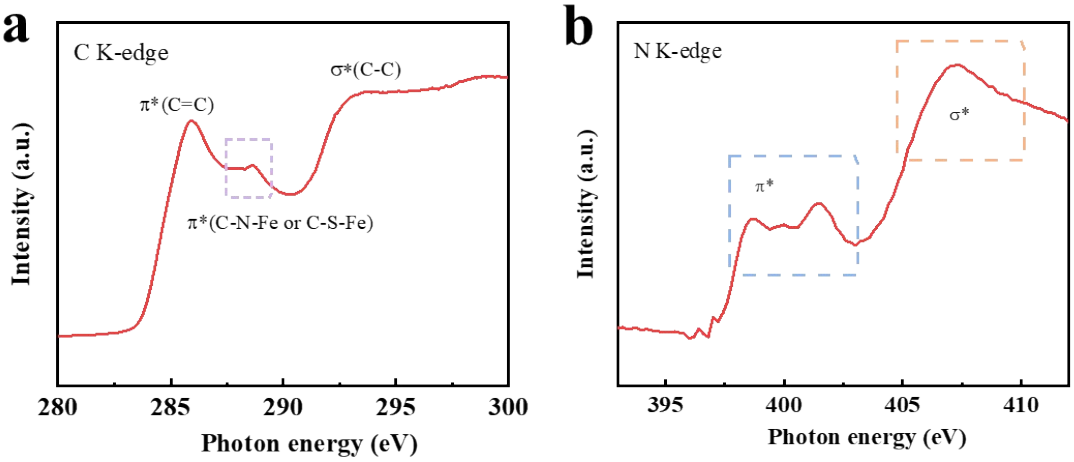

Fig S15. (a) C K-edge and (b) N K-edge XANES spectra of H-S-Fe-NC.

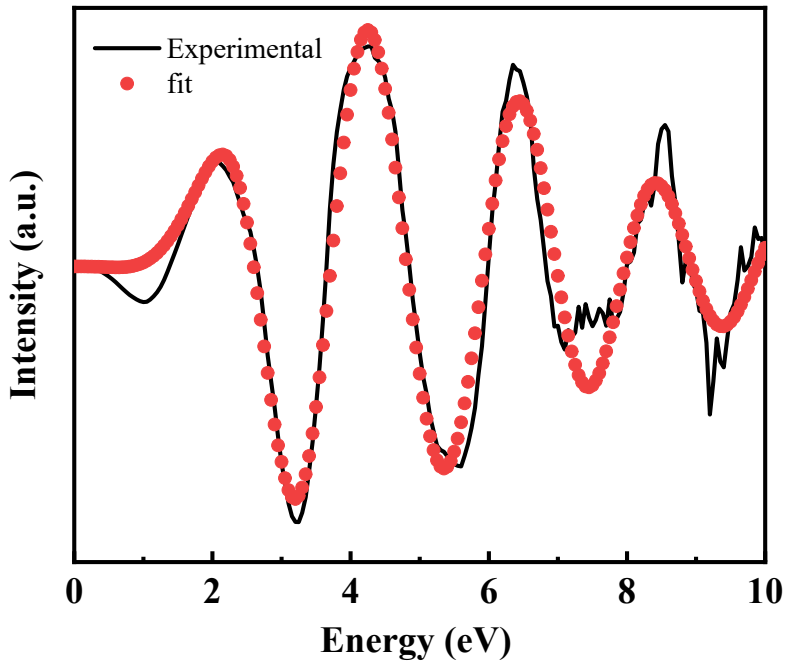

Fig S16. FT-EXAFS fitting curves of H-S-Fe-NC in K-space.

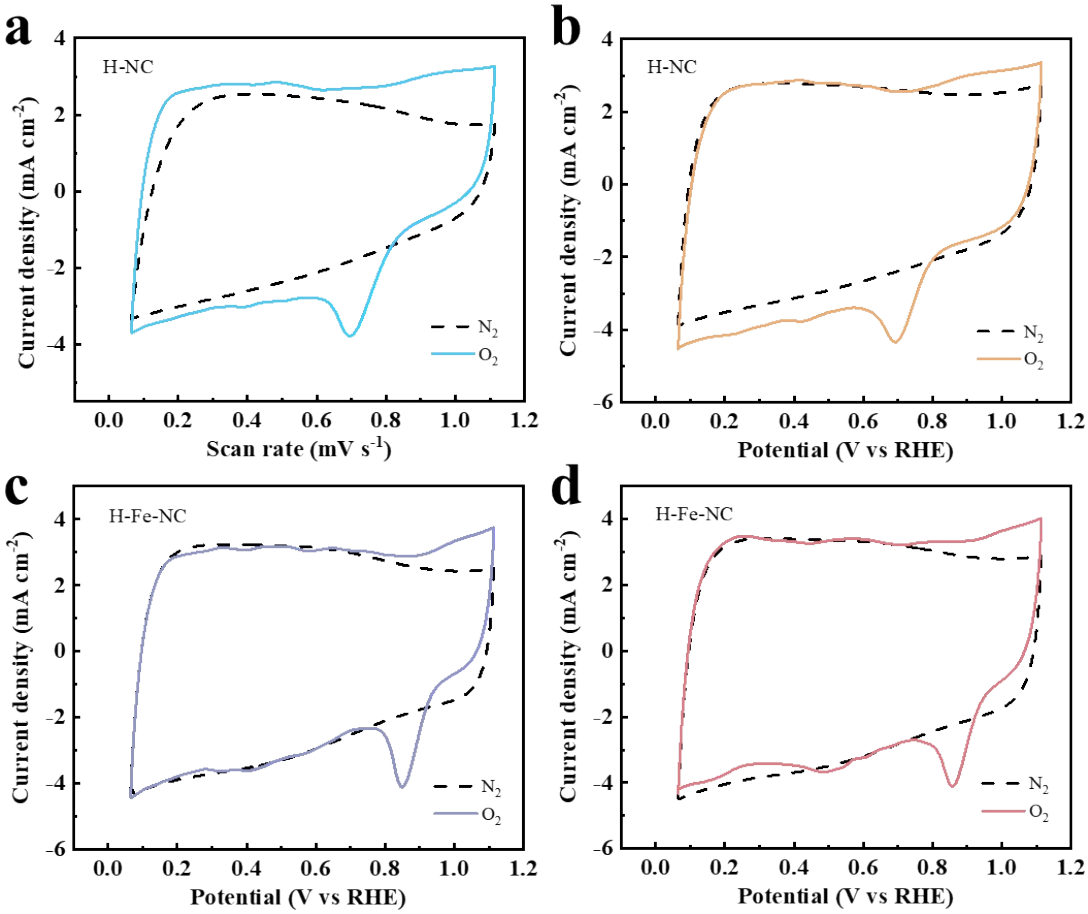

Fig S17. CV curves of H-NC, H-S-NC, H-Fe-NC and H-S-Fe-NC.

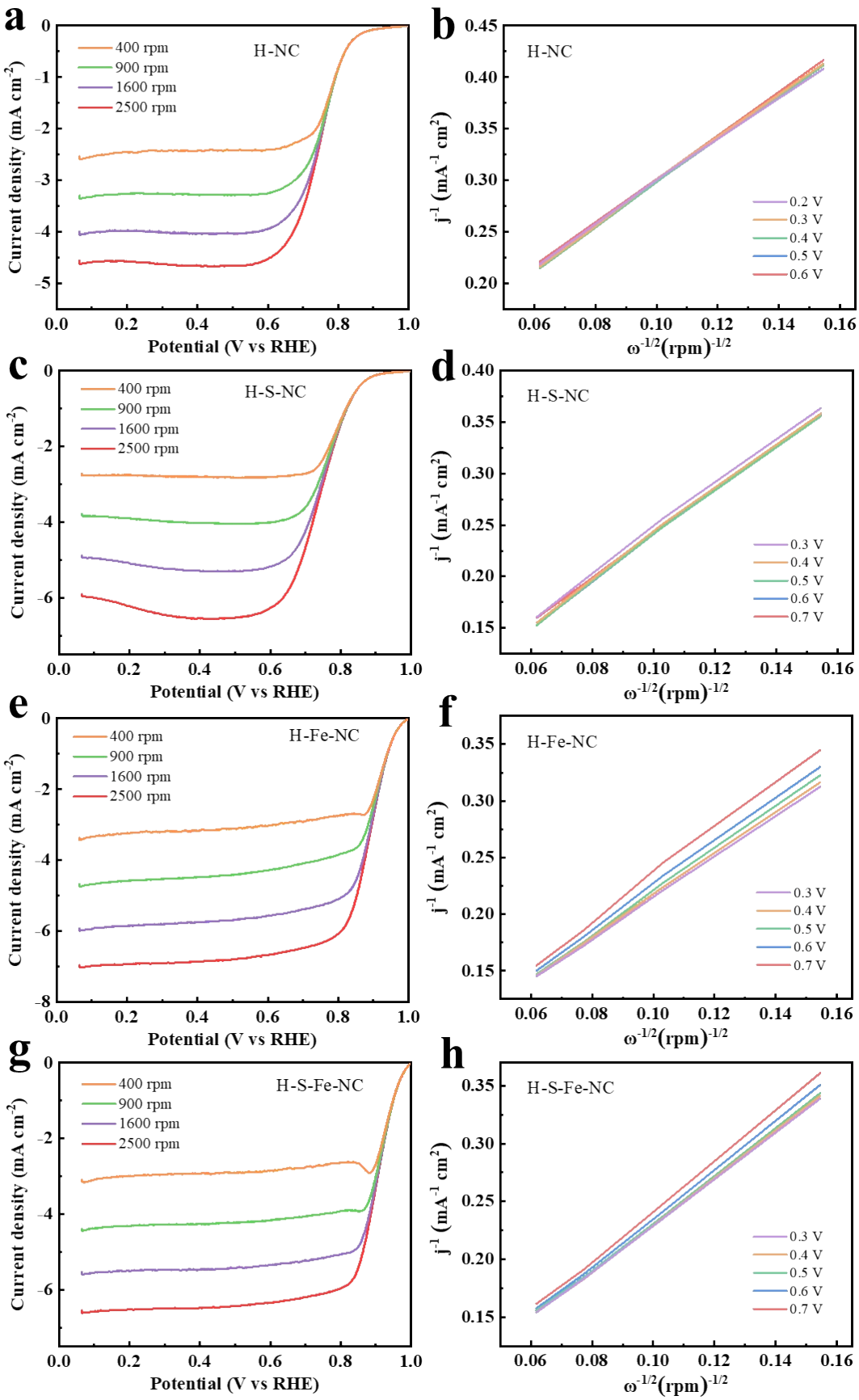

Fig S18. (a) Polarization curves and the corresponding K-L plots of (a-b) H-NC, (c-d) H-S-NC, (e-f) H-Fe-NC and (g-h) H-S-Fe-NC.

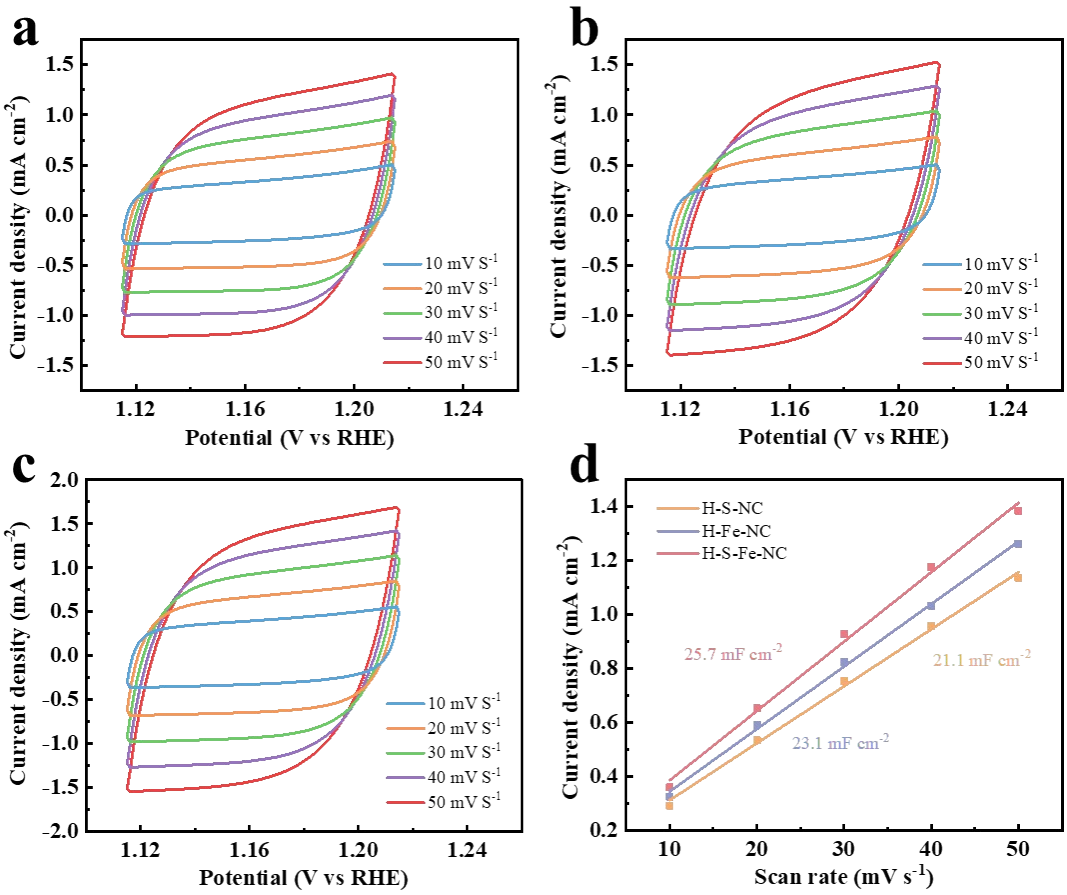

Fig S19. CV curves at scan rates from 10 to 50 mV s^{-1} and the corresponding linear fitting of capacitive current for H-S-NC, H-Fe-NC and H-S-Fe-NC.

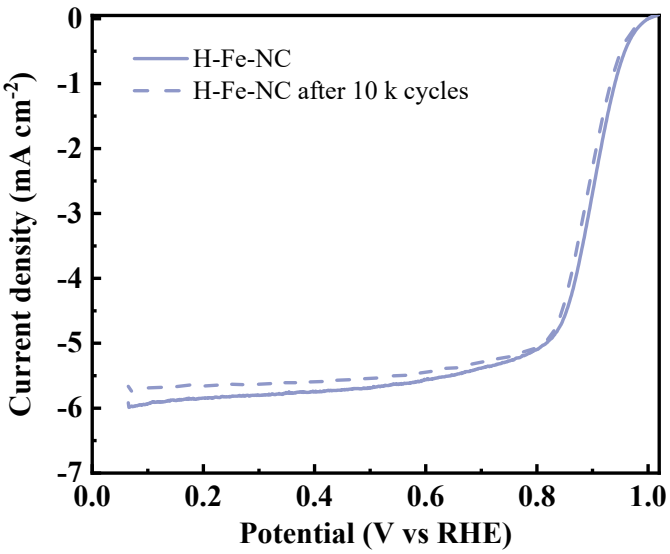

Fig S20. LSV curves of H-Fe-NC before and after 10 k cycles

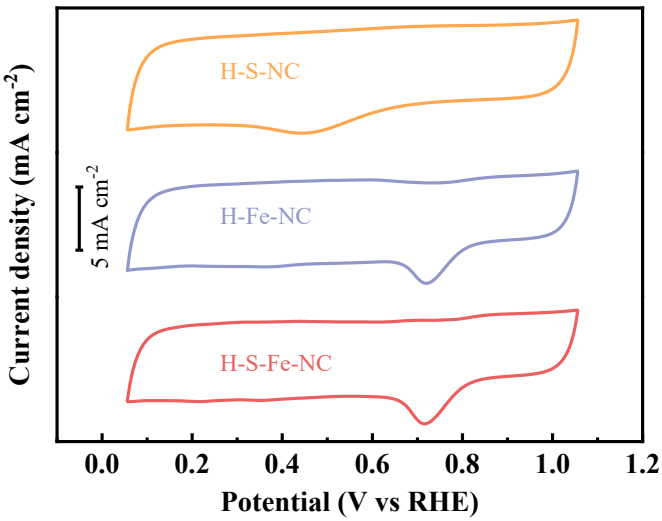

Fig S21. CV curves of H-S-NC, H-Fe-NC and H-S-Fe-NC under O_2 saturated 0.1M $HClO_4$.

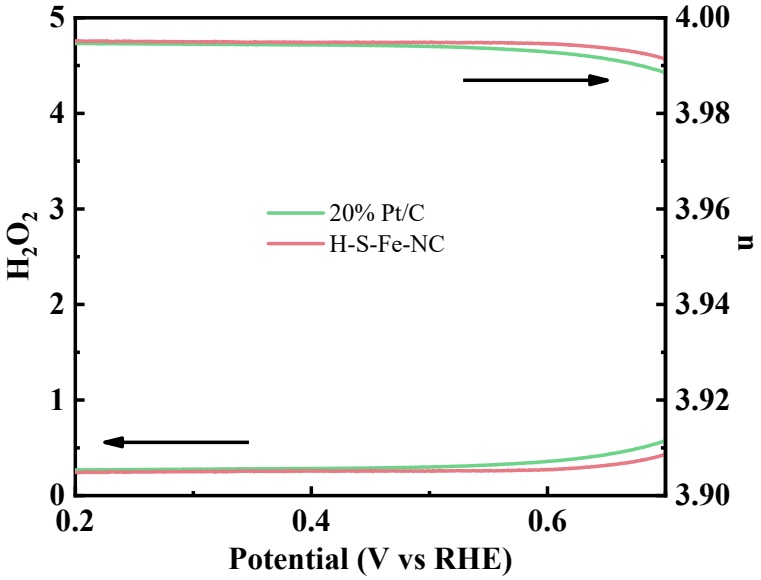

Fig S22. Electron transfer number (bottom) and H_2O_2 yield (top) of H-S-Fe-NC and 20% Pt/C in 0.1M $HClO_4$.

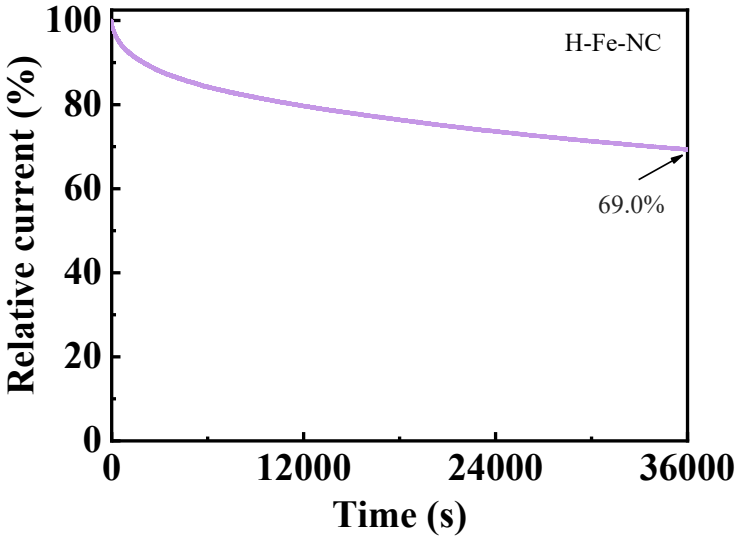

Fig S23. chronoamperometry respond of H-Fe-NC in 0.1M $HClO_4$.

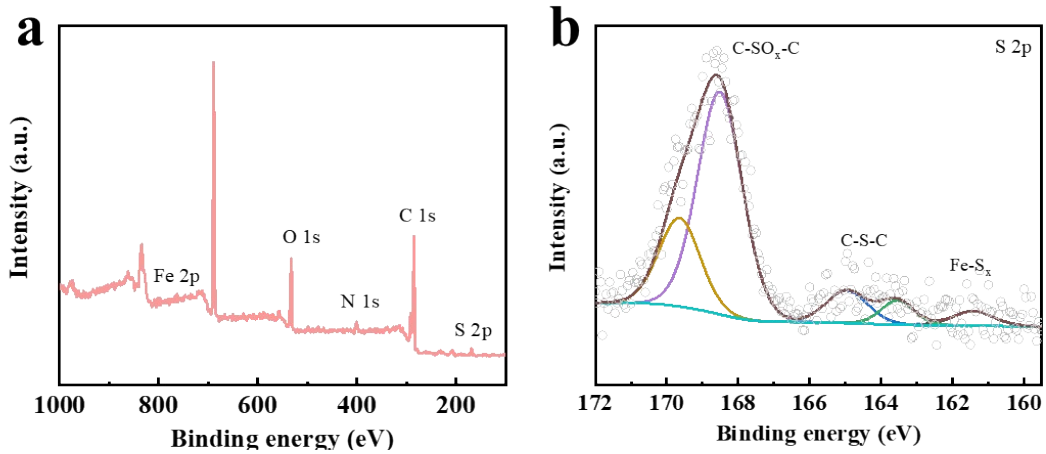

Fig S24. (a) the survey XPS spectrum and (b) high-resolution S 2p XPS spectra of H-S-Fe-NC after durability measurement.

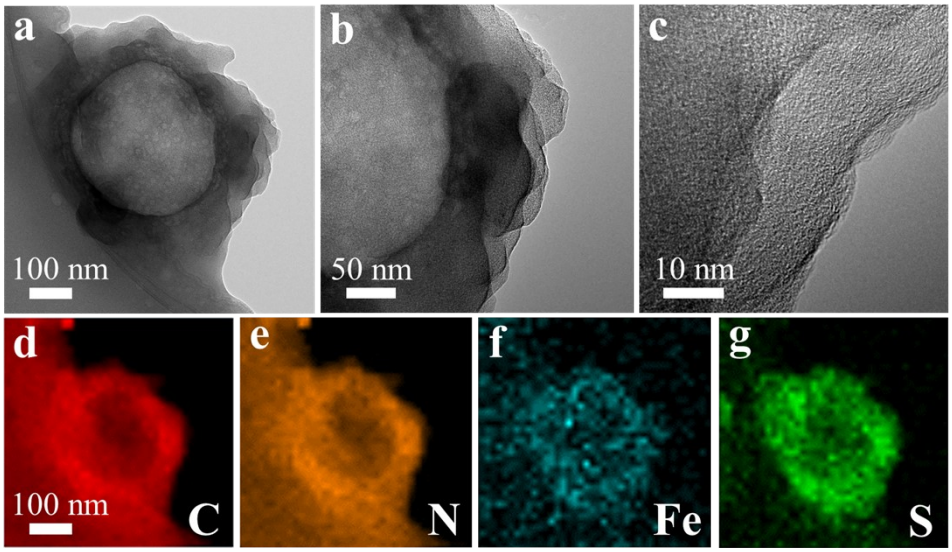

Fig S25. TEM image, HR-TEM image and elemental mappings of C, N, Fe, and S for H-S-Fe-NC after durability measurement.

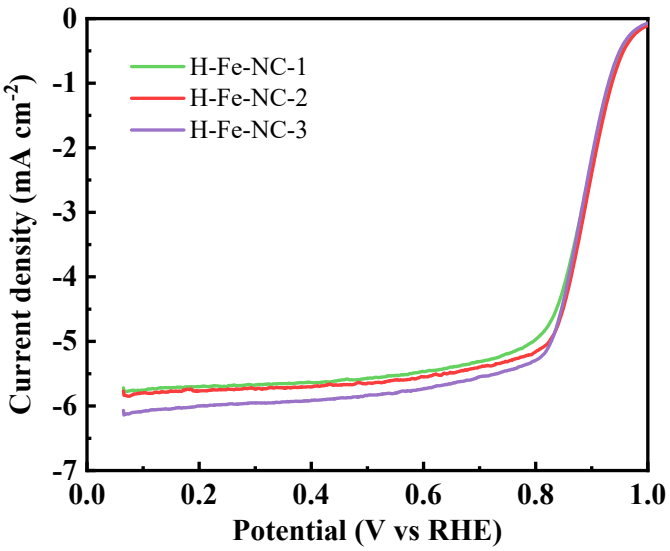

Fig S26. (a) ORR Polarization curves of H-Fe-NC with the different Fe content.

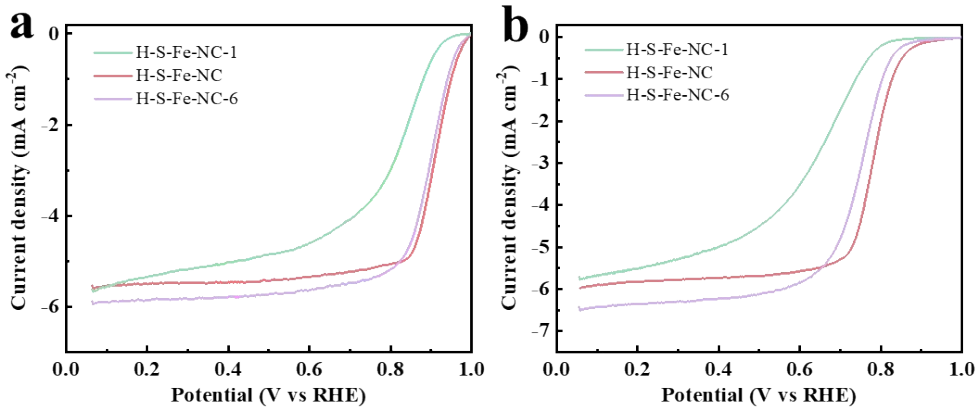

Fig S27. ORR Polarization curves of H-S-Fe-NC with the different ratio of thiourea in (a) 0.1 KOH solution and (b) 0.1M $HClO_4$ solution, respectively.

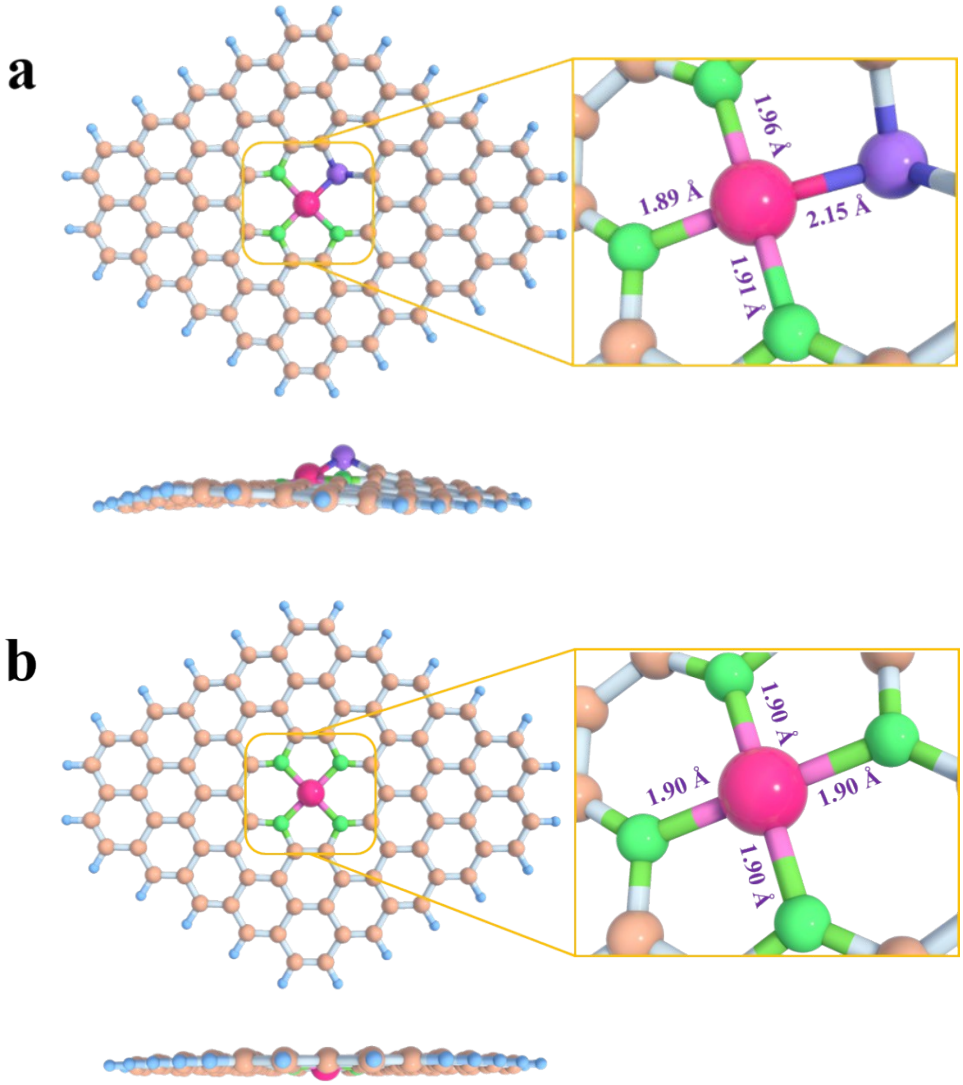

Fig S28. Optimized structure of (a) H-S-Fe-NC and (b) H-Fe-NC.

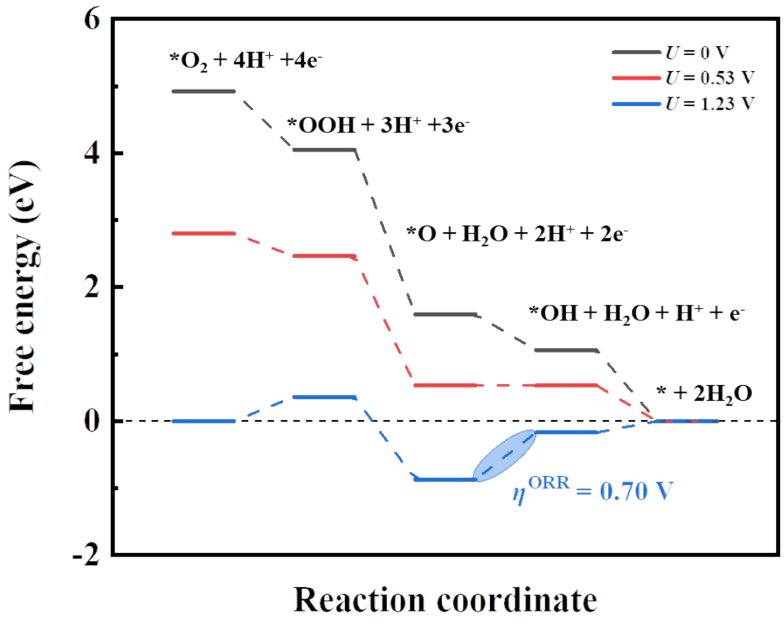

Fig S29. Gibbs free energy diagram of intermidiate on ORR of H-Fe-NC under acid condition.

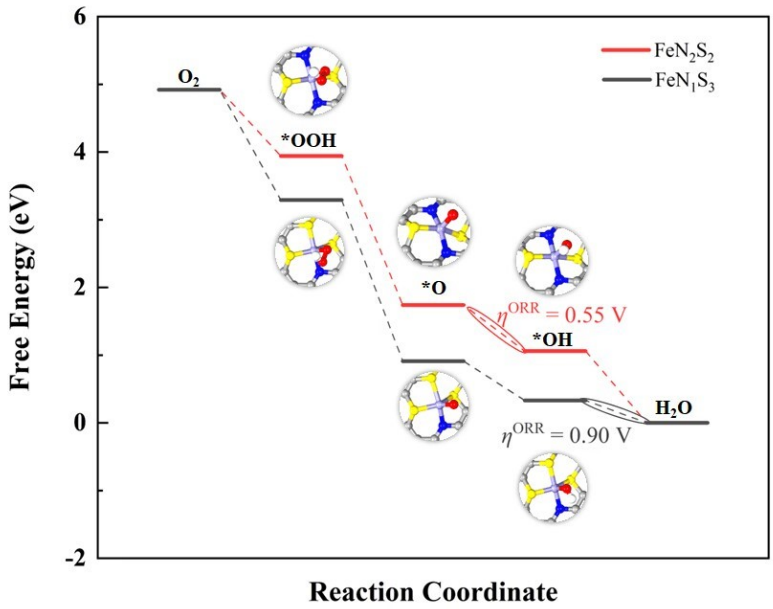

Fig S30. Gibbs free energy diagrams of ORR under acid condition on FeN_2S_2 and FeN_1S_3

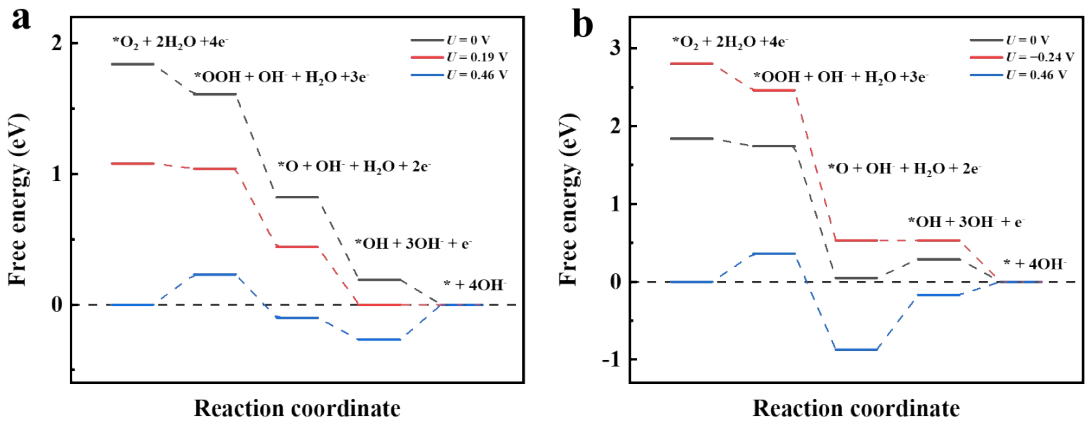

Fig S31. Gibbs free energy diagram of intermidiate on ORR of (a) H-S-Fe-NC and (b) H-Fe-NC under alkaline condition.

Table S1. BET surface area, total pore volume, and average pore size of synthesized catalysts.

sample	BET specific surface area(m^2 g^{-1})		Total pore volume (cm^3 g^{-1})		Average pore size (nm)	
	Mesopore	**Micropore**	**Mesopore**	**Micropore**	**Mesopore**	**Micropore**
H-NC	456.8	658.8	0.64	0.35	13.8	3.06-3.55
H-S- NC	294.3	475.4	0.37	0.25	14.1	
H-Fe-NC	442.6	746.1	0.56	0.39	12.4	
H-S-Fe-NC	333.0	555.4	0.39	0.29	13.5	

Table S2. The element content of the catalyst based on the XPS survey.

sample	C (at.%)	N (at.%)	O (at.%)	S (at.%)	Fe (at.%)
H-NC	86.66	9.09	4.24	0	0
H-S-NC	81.43	8.90	7.98	1.69	0
H-Fe-NC	89.67	4.87	5.37	0	0.1
H-S-Fe-NC	88.88	5.08	4.94	0.9	0.2

Table S3. The relative contents of different types of nitrogen species in the as-prepared samples obtained from XPS results.

sample	Pyridinic-N (%)	Fe-Nx (%)	Pyrrolic-N (%)	Graphitic-N (%)	N-oxide (%)
H-NC	60.6	0	9.1	22.4	7.9
H-S-NC	51.0	0	12.8	31.1	5.1
H-Fe-NC	45.0	10.3	5.8	32.0	5.7
H-S-Fe-NC	43.0	10.3	8.2	30.6	7.7

Table S4. Curve fit Parameters[a] for Fe K-edge EXAFS for the H-S-Fe-NC.

path	N	R(Å)	σ^2 (x10^{-3} Å^2)
Fe-N	3[b]	1.99	0.01
Fe-S	1[b]	2.38	0.04

[a] $S0^2$ was fitting as 1.0, the inner potential correction is (E_0) is -2.03 eV; The number of variable parameters is 5, R-factor for this fit is 0.002,

[b] These coordination numbers were constrained as N (Fe-S) = 1 and N (Fe-N) = 3 based on the standard structure.

Table S5. ORR performance of the as-synthesized catalysts in 0.1 M KOH

Sample	E_{onset} (V vs RHE)	$E_{1/2}$ (V vs RHE)	J_L (mA cm^{-2})	$J_{k\ 0.85\ V}$ (mA cm^{-2})
H-S-NC	0.938	0.751	4.02	0.22
H- Fe-NC	0.988	0.894	5.872	16.87
H-S-Fe-NC	0.995	0.910	5.484	42.03
Pt/C	0.990	0.873	5.65	10.53

Table S6. Comparison of ORR catalytic activities between H-S-Fe-NC and other well-developed Fe-based ORR electrocatalysts in 0.1 M KOH.

Sample	E_{onset} (V vs RHE)	$E_{1/2}$ (V vs RHE)	Ref.
Fe-N-C	1.06	0.904	Small 2018, 14, 1704282
Fe(Fc)-N/S-C	0.991	0.872	ACS Catal. 2021, 11, 7450-7459.
NP-Fe-NHPC	0.99	0.88	Adv. Mater. 2020, 1907399
VC-MOF-Fe	0.91	0.886	Nano Energy 2021, 82, 105714
Fe-ISA/SNC	-	0.89	Adv. Mater. 2018, 30, 1800588
Fe-N-C/N-OMC	1.08	0.93	Appl. Catal. B-Environ. 2021, 280, 119411
Fe/OES	1.0	0.85	Angew Chem. Int. Ed. 2020, 132, 7454
Fe-N-C HNSs	1.04	0.87	Adv. Mater. 2019, 31, 1806312.
Fe-Nx/HPC-1000	0.97	0.88	Chem. Eng. J. 2022, 429, 132214.
Fe-NC SAC	0.98	0.90	Nat. Commun. 2019, 10, 1278.
H-S-Fe-NC	**0.995**	**0.910**	**This work**

Table S7. ORR performance of the as-synthesized catalysts in 0.1 M $HClO_4$.

Sample	E_{onset} (V vs RHE)	$E_{1/2}$ (V vs RHE)	J_L (mA cm^{-2})	$J_{k\ 0.75\ V}$ (mA cm^{-2})
H-S-NC	0.805	0.451	5.07	0.15
H- Fe-NC	0.913	0.772	5.70	11.47
H-S-Fe-NC	0.921	0.782	5.77	18.12
Pt/C	0.891	0.728	5.55	3.77

Table S8. Formation energy (E_f) of FeN_1S_3, FeN_2S_2 and FeN_3S_1

Structure	E_f (eV)
FeN_1S_3	−0.71
FeN_2S_2	−0.55
FeN_3S_1	−0.40